

\*Corresponding author; email: egutsmie@e18.physik.tu-muenchen.de

## Density of states in solid deuterium: Inelastic neutron scattering study

A. Frei, E. Gutmiedl\*, C. Morkel, A.R. Müller, S. Paul, M. Urban

*Technische Universität München, Physik-Department,  
James-Frank-Str., D-85747 Garching, Germany*

H. Schober, S. Rols

*Institut Laue Langevin, 156X, F-38042 Grenoble CEDEX, France*

T. Unruh

*Technische Universität München, Forschungsneutronenquelle Heinz  
Maier-Leibnitz (FRM II), Lichtenbergstr. 1, D-85747 Garching, Germany*

M. Hölzel

*Technische Universität Darmstadt, Material-und Geowissenschaften,  
Petersenstr. 23, D-64287 Darmstadt, Germany*

(Dated: May 25, 2009)

## Abstract

The dynamics of solid deuterium ( $\text{sD}_2$ ) is studied by means of inelastic scattering (coherent and incoherent) of thermal and cold neutrons at different temperatures and para-ortho ratios. In this paper, the results for the generalized density of states (GDOS) are presented and discussed. The measurements were performed at the thermal neutron time-of-flight (TOF) instrument IN4 at ILL Grenoble and at the cold neutron TOF instrument TOFTOF at FRM II Garching. The GDOS comprises besides the hcp phonon excitations of the  $\text{sD}_2$  the rotational transitions  $J = 0 \mapsto 1$  and  $J = 1 \mapsto 2$ . The intensities of these rotational excitations depend strongly on the ortho- $\text{D}_2$  molecule concentration  $c_o$  in  $\text{sD}_2$ . Above  $E = 10$  meV there are still strong excitations, which very likely may originate from higher energy damped optical phonons and multi-phonon contributions. A method for separating the one- and multi-phonon contributions to the density of states will be presented and discussed.

PACS numbers: 28.20.Cz, 63.20.kk

Keywords: neutron, phonons, solid deuterium

## I. INTRODUCTION

Solid deuterium (sD<sub>2</sub>) and solid hydrogen are typical quantum molecular solids. Each D<sub>2</sub>/H<sub>2</sub> molecule exhibits large zero-point vibrations due to the small molecule mass. These quantum solids have been investigated theoretically [1] and by experimental techniques like inelastic neutron scattering [2] and Raman scattering [3]. Solid deuterium has an almost perfect hcp crystal structure, when it is prepared under suitable conditions [4] (low pressure and  $T > 5$  K). The phonon dispersion relation of solid ortho-deuterium (o-D<sub>2</sub>) was measured in the past by inelastic coherent neutron scattering [5]. These measured phonon dispersion relations are in good agreement with recent calculations based on molecular dynamics calculations (MDC) [1]. In the case of solid para-hydrogen, the molecular calculations [1] disagree to some extent with the experimental data of *Nielsen* [2]. The MDC predicts phonons above 10 meV in solid para-hydrogen, which did not appear in the neutron scattering measurements of *Nielsen* [2]. One possible explanation could be the restriction to energies below 9 meV in Nielsen's data analysis [1]. Recent inelastic incoherent neutron scattering data on solid para-hydrogen [6] are showing also excitations above 10 meV.

The D<sub>2</sub> molecule has internal rotational modes, which are described by the rotational quantum number  $J$ . In the solid phase,  $J$  is still a good quantum number. Deuterium in states with even  $J$  ( $J=0,2,4,\dots$ ) is termed ortho-deuterium (o-D<sub>2</sub>), whereas D<sub>2</sub> in states with odd  $J$  ( $J=1,3,5,\dots$ ) is termed para-deuterium (p-D<sub>2</sub>). At low temperatures ( $T \sim 6$  K), about 99.999% of the deuterium molecules are in the ortho state, when thermal equilibrium is reached. At room temperature, D<sub>2</sub> has an ortho concentration of 66.7%. After cooling down the D<sub>2</sub> to the solid phase ( $T \sim 6$  K), it normally takes months to reach the equilibrium of 99.999% o-D<sub>2</sub>. This process can be accelerated by using paramagnetic materials like chromium oxides or hydrous ferric oxides [7, 8, 9] as catalysts for the para-ortho conversion. With this kind of converters, it is possible to reduce the conversion time to below one day in typical experiments and to adjust the o-D<sub>2</sub> concentration between 66.7% and  $\geq 98\%$  for investigating in detail its influence on the structure and dynamics of solid deuterium.

Neutron scattering is an excellent tool to investigate the phonon system and the rotational transitions of D<sub>2</sub> molecules in sD<sub>2</sub>. Neutrons are scattered by D coherently ( $b_{\text{coh}} = 6.671$  fm) and also incoherently ( $b_{\text{inc}} = 4.04$  fm) [10]. Scattering of neutrons where a rotational transition ( $J \mapsto J'$ ,  $J \neq J'$ ) is involved, leads to an incoherent response of the system. The phonon excitations are present in the coherent part of the scattering, whereas the incoherent part is determined by rotational transitions and also by incoherent phonon scattering [11, 12].

In principle the cross section for neutron scattering in sD<sub>2</sub> is described by,

$$\frac{\partial^2 \sigma}{\partial \omega \partial \Omega} = \frac{k}{k_0} b_{\text{coh}}^2 S_{\text{coh}}(Q, \omega) + \frac{k}{k_0} b_{\text{inc}}^2 S_{\text{inc}}(Q, \omega). \quad (1)$$

Here,  $k_0$  is the wave number of the incoming neutron,  $k$  the wave vector of the scattered neutron,  $S_i(Q, \omega)$  ( $i = \text{coh}, \text{inc}$ ) are the dynamical structure functions of coherent and incoherent scattering, respectively. The energy change of the neutron is  $E = \hbar\omega$ , while  $\hbar Q$  is the momentum transfer. The coherent and incoherent scattering lengths are  $b_{\text{coh}}$  and  $b_{\text{inc}}$  respectively.

In the incoherent approximation the neutron scattering cross section Eq. (1) can be expressed by [13]:

$$\frac{\partial^2 \sigma}{\partial \omega \partial \Omega} = \frac{k}{k_0} [b_{\text{eff}}(Q)]^2 \frac{\hbar Q^2}{2M} \frac{G(\omega)}{\omega} [n(\omega) + 1] e^{-2W(Q)}. \quad (2)$$

The generalized density of states (GDOS)  $G(\omega)$  comprises the complete phonon excitations of sD<sub>2</sub> as well as rotational transitions of individual D<sub>2</sub> molecules. Furthermore, multi-phonon excitations of the phonon system of sD<sub>2</sub> [14] should appear in the GDOS, as they are not corrected for in Eq. (2). The term  $e^{-2W(Q)}$  is the well known Debye-Waller factor, where  $W(Q) = \frac{1}{6} Q^2 \langle u^2 \rangle$ , and  $\langle u^2 \rangle$  ( $\langle u^2 \rangle = 0.25 \text{ \AA}^2$ ) is the mean square displacement [5] of the D<sub>2</sub> molecule in the lattice. The quantity  $n(\omega)$  is the Bose statistic function, and  $[n(\omega) + 1]$  describes the creation of a boson, which causes the neutron energy loss. The scattering length  $b_{\text{eff}}(Q)$  is a combination of coherent and incoherent scattering lengths. This combination depends strongly on the rotational transitions excited by the neutrons [12] (see TABLE I).

Factorization (Eq. (2)) is only applicable, if the total scattering response of solid deuterium contains an essential amount of incoherent scattering (incoherent approximation), or if averaging over a sufficiently large  $Q$  range is performed. This is the case for thermal neutron scattering.

TABLE I: Neutron scattering lengths  $b$  associated with rotational transitions [12].

$J \mapsto \tilde{J}$	$E$ [meV]	$b^2$
$0 \mapsto 1$	7.0	$0.375 \, b_{\text{inc}}^2$
$1 \mapsto 2$	13.5	$0.75 \, b_{\text{inc}}^2$
$0 \mapsto 2$	21.0	$b_{\text{coh}}^2 + 0.625 b_{\text{inc}}^2$
$1 \mapsto 0$	7.0	$0.75 b_{\text{inc}}^2$

In principle,  $[b_{\text{eff}}(Q)]^2$  is expressed by

$$\begin{aligned}
[b_{\text{eff}}(Q)]^2 = & (1 - c_p) \cdot \left[ 4 \left( b_{\text{coh}}^2 + \frac{5}{8} b_{\text{inc}}^2 \right) j_0^2(Q a_s / 2) \right] \\
& + (1 - c_p) \cdot \left[ \frac{9}{2} b_{\text{inc}}^2 (j_1^2(Q a_s / 2)) \right] \\
& + c_p \cdot [3 b_{\text{inc}}^2 (2 j_1^2(Q a_s / 2) + 3 j_3^2(Q a_s / 2))] \\
& + c_p \cdot [4 b_{\text{coh}}^2 + b_{\text{inc}}^2 (j_0^2(Q a_s / 2) + 2 j_2^2(Q a_s / 2))] ,
\end{aligned} \tag{3}$$

where  $j_i(Q \cdot a_s / 2)$  are the spherical Bessel functions of order  $i$ . The first term in Eq. (3) describes the transition  $J = 0 \mapsto 0$  (even-even), while the second term the  $J = 0 \mapsto 1$  (even-odd) transition. The third and fourth term take the  $J = 1 \mapsto 2$  (odd-even) and  $J = 1 \mapsto 1$  (odd-odd) transition into account. The parameter  $a_s = 0.74 \, \text{\AA}$  is the distance of the deuterons within the  $\text{D}_2$  molecule [5], while  $c_p$  is the concentration of the molecules in the para state ( $c_p + c_o = 1$ ,  $c_o$  is the concentration of molecules in the ortho state).

With the measured inelastic neutron cross section and Eq. (2), it is possible to determine the GDOS. The GDOS for differently prepared sD<sub>2</sub> crystals with different ortho

concentrations are the main subject of this paper. Furthermore, a method of extracting the density of states of one-quasi-particle excitations  $G_1(E)$  from our data is presented. A detailed analysis of the dynamical and static structure of solid deuterium will be presented in a forthcoming publication.

## II. EXPERIMENTAL DETAILS

The experiments on inelastic neutron scattering were performed at the Time-Of-Flight (TOF) spectrometer for thermal neutrons IN4 [15] of the Institute Laue-Langevin (ILL), Grenoble, France and at the cold TOF spectrometer TOFTOF [16] at FRM II, Garching, Germany.

The measurements at IN4 were carried out at two different wavelengths of the incoming neutrons ( $\lambda \simeq 2.2 \text{ \AA}$  and  $1.1 \text{ \AA}$ ). The energy resolution for the two different wavelengths had been determined to be  $\Delta E_{2.2} = 0.7 \text{ meV}$  and  $\Delta E_{1.1} = 3.4 \text{ meV}$ , using the standard technique of elastic neutron scattering on a vanadium sample.

The IN4 spectrometer supplies a typical thermal neutron flux of  $5 \cdot 10^5 \text{ cm}^{-2} \text{ s}^{-1}$  on the sample. The beam size on the sample is  $\sim 2 \times 4 \text{ cm}^2$ . The scattering angle  $2\theta$  varies between  $13^\circ$  and  $120^\circ$ . The beam divergence is  $\Delta\theta = 1^\circ$ .

The sample cell for the solid deuterium was designed and constructed to fit into the standard "orange cryostat" of ILL [17]. The sample cell is cooled down to the desired temperature by using an exchange gas (helium) in the chamber which surrounds the sample cell. The cooling inside the cryostat is done by a liquid-nitrogen shield and a liquid-helium heat exchanger. Neutron scattering on solid/liquid deuterium was performed at temperatures between  $T = 3.5 \text{ K}$  and  $T = 23 \text{ K}$ . The temperature stability was better than  $0.1 \text{ K}$ .

The  $\text{sD}_2$  is frozen inside the double-wall cylinder volume (see Fig. 1). The thickness of the  $\text{sD}_2$  in the cell is fixed to  $\delta = 2 \text{ mm}$ . The attenuation of the incoming thermal neutrons ( $E_0 \sim 17 \text{ meV}$ ) in the filled sample cell is  $\sim 25\%$ , and therefore multiple neutron scattering inside the sample can not be neglected. The influence of multiple scattering will

be discussed in detail in the section "Results and discussion". The sample cell is connected to the D<sub>2</sub> gas handling system via a 12 mm×1 mm stainless steel pipe.

The gas handling system is especially designed to keep the pressure of the D<sub>2</sub> gas flow into the sample cell quasi-independent of the temperature within the cell. This is done by using needle valves for the gas flow. With this technique, it is possible to follow a special path in the phase diagram (see Fig. 2) of D<sub>2</sub>. This can be either the path from the gas via the liquid to the solid phase, or the path directly from the gas to the solid phase (sublimation). The triple point of D<sub>2</sub> is at [ $T_t = 18.7$  K,  $P_t \sim 180$  mbar]. At pressures below  $P_t$ , direct sublimation of D<sub>2</sub> is possible, while at pressures above  $P_t$ , the D<sub>2</sub> is liquefied before it becomes a solid.

The para-to-ortho converter [9], which accelerates the conversion from the p-D<sub>2</sub> to o-D<sub>2</sub> state (Fig. 3), is attached to the gas handling system via a stainless-steel pipe. This converter is an independent cryogenic system, cooled by a cold finger. The main part of this system is a copper cup, filled with a paramagnetic powder. This powder was extracted from an OXISORB [9] unit, which is normally a gas cleaning tool. OXISORB contains paramagnetic chromium composition, which acts inside the converter as a catalyst. The upper part of the copper cup is closed by a sinter disc, which keeps the powder in the cup, but is permeable to D<sub>2</sub> gas. This copper cup is mounted on the finger of the cooling machine, and can be operated between  $T = 10$  K and room temperature. During the filling mode, the cup is fed with D<sub>2</sub> gas from the gas handling system. The D<sub>2</sub> is liquified inside the cup, and is kept there at the boiling point for the necessary conversion time (hours). Keeping the liquid at the boiling point shortens the conversion time considerably (factor 2) [9].

The filling procedure of the sample cell was monitored with the help of the IN4 spectrometer. Filling was stopped when the scattered-neutron intensity reached its maximum and stayed constant. This method was used for filling natural deuterium gas from the dump and also for filling the converted deuterium gas from the converter unit.

The experiments at TOFTOF of FRM II were performed with an equipment similar to that used at IN4. These experiments were performed before the IN4 experiment and

served to optimize the sample cell for the IN4 experiment. Sample cell and cooling machine at the TOFTOF experiment were different from the setup at IN4. The thickness of the sD<sub>2</sub> in the cell was bigger than that ( $\delta = 3$  mm) in the IN4 sample cell. The attenuation of the incoming thermal neutrons ( $E_0 \sim 20$  meV,  $\lambda \simeq 2.0$  Å) in the filled sample cell is  $\sim 30\%$ , and therefore multiple neutron scattering inside the sample can not be neglected. The influence of multiple scattering will be discussed in detail in the section "Results and discussion". Later, after the IN4 experiment, a second experiment was done with sD<sub>2</sub> at the TOFTOF, in order to improve the statistics of neutron data for energy transfers larger than 10 meV.

The sample cell at TOFTOF is cooled by a closed cycle cold-head machine with He exchange gas. With this setup temperatures down to  $T \sim 7$  K were reached. The measurements at TOFTOF were carried out at three different wavelengths of the incoming neutrons ( $\lambda \simeq 2.0$  Å,  $\lambda \simeq 2.6$  Å and  $\lambda \simeq 6.0$  Å). The energy resolution for the different wavelengths has been determined to  $\Delta E_{2.0} = 1.23$  meV,  $\Delta E_{2.6} = 0.74$  meV and  $\Delta E_{6.0} = 0.07$  meV, using the standard technique of elastic neutron scattering on a vanadium sample.

At TOFTOF the typical cold neutron flux on the sample amounts to  $7 \cdot 10^4$  cm<sup>-2</sup> s<sup>-1</sup>. The beam size on the sample is  $\sim 3 \times 5$  cm<sup>2</sup>. The TOFTOF detector bank covers a range of  $2\theta = 7.5^\circ \dots 140^\circ$ . The beam divergency is  $\Delta\theta \sim 1^\circ$ .

### III. SAMPLE PREPARATION

The structure and dynamics of sD<sub>2</sub> may be influenced by the way of preparing the crystals [18, 19]. Therefore samples of different character were prepared by different freezing procedures. Our own experiments had shown differences in the optical quality of D<sub>2</sub> for different freezing procedures (see Fig. 4).

Freezing experiments with p-sH<sub>2</sub> and o-sD<sub>2</sub> films on MgF<sub>2</sub> coated sapphire plates [19] showed very interesting features concerning the microscopic and mesoscopic structure of solid deuterium and hydrogen films. Below  $T_d < 6$  K (deposition temperature) a mixture of hcp and fcc structures is possible in the sD<sub>2</sub> film. The fcc component disappears if the temperature is raised above 9.5 K (annealing). The remaining hcp structure is preserved, even if the temperature is lowered again below 9.5 K. These observations were



one motivation to look for a possible influence of the freezing procedure on the structure and dynamics of sD<sub>2</sub>. The following freezing procedures were applied:

**Liquid-Solid (LS):** D<sub>2</sub> is liquefied in the sample cell at  $T \sim 21$  K. The filling is monitored by neutron scattering measurements at IN4. After filling, the temperature of the cooling controller is lowered to a temperature slightly below  $T = 18.7$  K and kept constant, the sample starts to freeze slowly. The sD<sub>2</sub> sample is then cooled down slowly to the desired measurement temperature. Slow cooling of the sD<sub>2</sub> is necessary to avoid sudden cracking of the solid deuterium.

**Liquid-Solid-Melt-Solid (LSMS):** An alternative method of producing good samples of sD<sub>2</sub> is remelting the solid at  $T = 18.7$  K. When the solid is melting, a mixture of liquid and small pieces of solid deuterium crystals will emerge. The character of this mixture can be monitored by neutron-scattering measurements. The static structure factor indicates the crossover from solid/liquid to complete liquid. The basic idea of this method is to stop the melting shortly before all solid pieces of sD<sub>2</sub> disappear. The remaining solid fragments serve as crystallization seeds for a new solid-deuterium sample.

**Gas-Solid (GS):** The re-sublimation of deuterium from gas is done by keeping the sample-cell temperature at  $T \sim 7 - 9$  K and maintaining a constant gas flow. With this method it is possible to grow slowly a solid-deuterium sample in the cell. How far the cell is filled with solid material is again monitored by neutron-scattering measurements.

**Turbo Solid (TS):** Fast freezing of sD<sub>2</sub> from the liquid phase at a temperature below  $T \sim 10$  K is leading to an opaque solid-deuterium sample (see Fig. 4c). The analysis of the static structure, extracted from the neutron scattering data, shows an almost ideal powder diffraction pattern for this "turbo solid". A detailed analysis of the structure of sD<sub>2</sub> will be presented in a forthcoming paper.

#### IV. RESULTS AND DISCUSSION

The TOF data were corrected for the empty-cell measurements, and normalized to the incoming flux and the vanadium standard. Based on this data the GDOS were determined by the IN4 computer code **gdos**. This code is implemented in the data analysis package LAMP [20], which is used for treating the data obtained from neutron scattering experiments at ILL. The basic method of this calculation is a sampling over a large  $Q$  range (neutron energy loss side), using the incoherent approximation [21] and referring to Eq. (2).

The GDOS is calculated by:

$$GDOS(\omega) = \omega \cdot \frac{S(Q(< 2\theta >), \omega)}{Q^2 \cdot (n + 1)} \quad (4)$$

The term  $Q(< 2\theta >)$  is a  $Q$  value for each energy transfer  $\hbar\omega$  considering an averaged scattering angle  $< 2\theta >$ . This simple approximation for the GDOS is commonly not equal to the real density of states (DOS). In many cases the agreement between the GDOS and DOS is remarkable. The GDOS incorporates the one-phonon and multi-phonon excitations. In the first order it is not so easy to separate the one-phonon part from the multi-phonon part. Nevertheless the GDOS is a useful tool to investigate the spectrum of excitations of the sample.

The experimental values of the GDOS for natural deuterium (o-D<sub>2</sub> 66.7%) in the liquid and also in the solid phase for different preparation methods of the crystals are shown in Fig. 5. The data for almost pure ( $c_o = 95\%$ ) o-D<sub>2</sub> are shown in Fig. 6.

The GDOS for differently prepared crystals at the same o-D<sub>2</sub> concentration does not show variations, beyond statistical effects. It seems that the way of preparing the crystals does not change the spectra of phonon excitations in sD<sub>2</sub>. The main difference between the GDOS for different o-D<sub>2</sub> concentrations is the strength of the rotational transition  $J = 0 \mapsto 1$ . Increasing the o-D<sub>2</sub> concentration enhances this transition. The GDOS shows for both o-D<sub>2</sub> concentrations a peak at  $E = 12..13$  meV. Furthermore, at  $c_o = 66.7\%$  there is a hint for the rotational transition  $J = 1 \mapsto 2$ . This excitation is not visible for  $c_o = 95\%$ .

An example for the influence of the o-D<sub>2</sub> concentration  $c_o$  on the rotational transitions is shown in Fig. 7. These data are taken from the later TOFTOF measurements ( $\lambda \simeq 2.0$  Å).

It is evident that increasing  $c_o$  leads to a larger cross section for the  $J = 0 \mapsto 1$  transition and also to a decrease of the  $J = 1 \mapsto 0$  transition.

The main focus of the data analysis presented here is the extraction of the density of states (DOS)  $G_1(E)$  of phonons and rotational transitions in solid  $D_2$  ("quasi particle picture"). The basic idea is to compare the integral over the scattering angle of the neutron scattering data  $d\sigma/dE_f$  with a calculated neutron cross section, using the incoherent approximation developed by *Turchin* [22] for a cubic crystal with one atom in the primitive cell. With the aid of this theory, it is possible to calculate the one-phonon and multi-phonon contributions to the neutron cross section  $d\sigma/dE_f$ , if  $G_1(E)$  is known.

This approach is only valid, if the detected neutrons are scattered neutrons from all possible directions of the first Brillouin zone in the crystal. This is normally the case, if one has a powder sample of the crystals. The diffraction pattern of fast frozen deuterium (TS,  $c_p=33.3\%$ ,  $T=9.5K$ ) shows an powder like behavior, although some small texture effects are visible (see Fig. 8). A Rietveld fit on this diffraction pattern gives the right values [23] for  $a$  and  $c$  of a hcp solid deuterium crystal ( $a = 3.596 \pm 0.005 \text{ \AA}$ ,  $c = 5.860 \pm 0.009 \text{ \AA}$ ). The positions of the different Bragg peaks correspond to a hcp solid  $D_2$  crystal. The fit-model contains also the Debye-Waller factor, because at larger scattering angles (higher  $Q$ -values) the scattering intensity is significantly reduced. The fit result for the mean square displacement  $\langle u^2 \rangle = 0.208 \pm 0.011 \text{ \AA}^2$  is smaller compared to value reported by *Nielsen* [5]. These results induced the decision to use only data from TS samples (second TOFTOF measurement) to determine the density of states  $G_1(E)$ .

$$\sigma_s(E_i \rightarrow E_f) = \sum_{n=1}^{\infty} \sigma_n(E_i \rightarrow E_f), \quad (5)$$

$$\frac{d\sigma_n}{dE_f} = \sigma_0(Q) \left(1 + \frac{1}{\mu}\right)^2 \sqrt{\frac{E_f}{E_i}} \frac{f_n(\epsilon)}{n!} F_n(E_i, E_f). \quad (6)$$

$$\sigma_0(Q) = 4\pi \cdot [b_{\text{eff}}(Q)]^2 \quad (7)$$

The summation over the index  $n$  (number of quasi particles involved in the scattering) contains all higher-order multi-quasi-particle excitations like multiphonons. With  $E_i$  and  $E_f$  are the energy of the incoming and outgoing neutron in the scattering process, respectively,

$\mu$  is the mass number of the D<sub>2</sub> molecule ( $\mu = 4$ ) and  $\epsilon$  is the energy transfer ( $E = E_i - E_f$ ) to the scattered neutron.

$$f_n(E) = \int_{-\infty}^{+\infty} f_{n-1}(E') f(E - E') dE', \quad (8)$$

$$f(E) = \frac{G_1(|E|)}{E(1 - e^{-E/k_B T})} \quad (9)$$

The function  $f(E)$  (see (Eq. (9))) contains the density of states  $G_1(E)$ , and it is possible to calculate the higher order functions  $f_n(E)$  with the help of Eq. (8).

$$F_n(E_i, E_f) = \frac{\mu}{4\sqrt{E_i E_f}} \int_{(\sqrt{E_i} - \sqrt{E_f})/\mu}^{(\sqrt{E_i} + \sqrt{E_f})/\mu} x^n e^{-x/\tau} dx \quad (10)$$

$$\tau = \left( \int_0^\infty \frac{1}{E} \coth\left(\frac{E}{2k_B T}\right) G_1(E) dE \right)^{-1} \quad (11)$$

In Eq. (10)  $F_n(E_i, E_f)$  is a kinematic factor, resulting from the integration over all angles in the neutron scattering process. The quantity  $\tau$  is the average energy of the excitations (mainly phonons) in sD<sub>2</sub>.

The starting point of the determination of  $G_1(E)$  is a first-guess model for  $G_1(E)$ , which should contain the phonons as well as the rotational transition  $J \mapsto J'$ . Following the approach of *Yu et al.* [24] a model with seven Gaussian functions is used to parameterize  $G_1(E)$ . The contribution of the three-particle excitations ( $d\sigma_3/dE_f$ ) was approximated by an additional Gaussian function.

$$G_1(E) = \sum_{l=1}^7 \alpha_l \frac{1}{\sqrt{2\pi}\sigma_l} e^{-\frac{1}{2} \frac{(E - \epsilon_l)^2}{(\sigma_l)^2}} \quad (12)$$

Treating phonons and rotational transitions as independent excitations may be not strictly correct in the calculation of the multiphonon contribution, but an eventual correction would occur at the far end of the energy spectrum above  $E > 14$  meV, which is not crucial important here.

The neutron cross section  $d\sigma/dE_f$  is calculated with Eqs. (5) - (12) and compared with the measured  $N_0 \cdot d\sigma_D/dE_f$  ( $N_0$  is a normalization factor). The parameters  $[\alpha_l, \sigma_l, \epsilon_l; l = 1..7]$  are determined by minimizing the difference between measured and calculated cross section.

Multiple scattering is in the case of the TOFTOF measurement not negligible. The deuterium sample scatters approximately 25% of the incoming beam. The scattering intensity is 50% elastic and 50% inelastic. The contribution of multiple scattering is a flat falling background ( $E > 3$  meV) and peak-like at  $E \sim 0$  meV. The multiple scattering was calculated (convolution of the scattering model with itself) by using the experimental deduced  $G_1(E)$  and applying the *Turchin* theory for one- and two-phonon neutron cross section. The magnitude (13%) of the multiple scattering was determined by using the work of *V.F. Sears* [25] ("rule of thumb" [26]). The flat falling background is smooth and has almost no texture. This background was included in the fit model, and cross checked afterwards with the convolution of  $d\sigma/dE$  with itself. The magnitude of multiple scattering, deduced from the fit must be in the same order, as predicted by the "rule of thumb"-estimation.

The TOFTOF measurements (see Fig. 9) clearly show the onset of two-particle contributions above  $E \sim 5$  meV and also one-particle excitations above  $E = 10$  meV. The TOFTOF data indicates three-particle excitations above  $E = 12$  meV. The peak at  $E = 5$  meV obviously originates from TA-phonons [2], whereas the peak at  $E \sim 7.5$  meV is a signature of the rotational transition  $J = 0 \mapsto 1$ .

Figure 10 shows the result for the one-particle density of states for solid  $D_2$  at  $c_o = 66.7\%$  and  $c_o = 98\%$  (area normalized to 1). Part a) of Fig. 10 shows the convoluted  $G_1(E)$ , while in part b)  $G_1(E)$  is de-convoluted with an Gaussian pseudo-resolution function with an  $FWHM = 1.0$  meV. This value was deduced from the  $FWHM$  of the elastic peak of  $d\sigma/dE$ .

The influence of the ortho concentration  $c_o$  on the density of states  $G_1(E)$  manifests itself (Fig. 10) in the expected enhancement of the peak at  $E \sim 7.5$  meV for larger  $c_o$ . Increasing the number of ortho molecules in solid  $D_2$  leads to a higher probability for  $J = 0 \mapsto 1$  transition. The position of the  $J = 0 \mapsto 1$  transition depends slightly on the concentration of para molecules  $c_p$  in the  $sD_2$ . A larger  $c_p$  lowers the  $J = 0 \mapsto 1$  energy ( $\delta E \sim 0.3$  meV for  $c_p = 33.3\%$ ). This energy shift can be explained by the interaction between p- $D_2$  ( $J = 1$ ) and o- $D_2$  molecules ( $J = 0$ ) [4].

The DOS derived from our measurements differs remarkably from earlier published results [24], which used the phonon dispersion measurements of *Nielsen* [5] to calculate the DOS of solid  $D_2$ . The DOS published by *Yu et al.* [24] contains pronounced peaks at 5 meV and 9 meV, which were identified with the acoustic and optical phonons in the hcp crystal. The

$J = 0 \mapsto 1$  transition was not considered by *Yu et al.* [24], and the DOS vanishes above 10 meV. The optical phonon contribution of the actually measured DOS for  $c_p=33.3\%$  seems to be smeared-out in the region of 8 – 12 meV, and does not peak at  $\sim 9$  meV, as it was published by *Yu et al.* [24]. This behavior was already observed in solid hydrogen by incoherent neutron scattering of *Bickermann et al.* [27] and *Colognesi et al.* [28]. *Bickermann et al.* explain the smearing-out of the higher-energy optical phonon groups by the anharmonicity of the quantum-crystal solid  $H_2$ . This anharmonicity leads to larger phonon line widths at higher energies. The DOS of *Colognesi et al.* shows at  $E \sim 9-10$  meV a small bump, which could be identified as optic phonons in solid hydrogen. In the case of almost pure o- $D_2$  ( $c_p=2\%$ ) a peak at  $E \sim 9$  meV in the DOS was found in the fit of our data. The amplitude of this optical peak is smaller than as it was published by *Yu et al.*. The appearance of multiphonons above 5 meV in our measurements leads to considerable line widths of the phonon groups above this certain energy. *Nielsen's* DOS was determined by a pseudoharmonic theory, which takes care of the renormalization of the phonon energies, but does not consider the change of the phonon line widths [27].

A second new feature of the result for  $G_1(E)$  presented here is a clear peak-like structure at  $E \sim 12$  meV. The intensity of this peak is more pronounced at higher  $c_o$ . This peak might be caused by the excitation of a combination of the rotational transition  $J = 0 \mapsto 1$  ( $\sim 7.5$  meV) and phonons with  $\sim 5$  meV energy. The DOS for phonons with  $\sim 5$  meV is very large. A combined excitation of phonons and rotational transitions of the  $D_2$  molecules is certainly a result of the interaction of the rotational transitions with the lattice of the solid  $D_2$  crystal (phonon-rotation coupling) [29]. A higher energy phonon ( $E > 12$  meV) is able to excite a low energy phonon and also the rotational transition  $J = 0 \mapsto 1$  through the phonon-rotation coupling. This decay of higher-energy phonons was maybe seen in our data. This peak could be on the other hand maybe an artefact, resulting from the incomplete separation of the one-particle-excitations and two-particle-excitations in the DOS, and has to be further investigated.

The DOS of solid  $D_2$  with higher para concentration ( $c_p = \sim 33.3\%$ ,  $c_o \sim 66.7\%$ ) contains a peak structure (see Fig. 10) at  $\sim 14$  meV, which is originated by the rotational transition  $J = 1 \mapsto 2$ . This peak is not seen at  $c_p = 2\%$ ,  $c_o = 98\%$ . This effect is obvious, because the  $J = 1 \mapsto 2$  transition scales with the number of para molecules in the solid  $D_2$ .

The result for  $G_1(E)$  derived from our neutron scattering data can be used to calculate

the mean square displacement  $\langle u^2 \rangle$ . This value ( $\langle u^2 \rangle = 0.22 \text{ \AA}^2$  for  $c_o \sim 66.7\%$ ) is quite close to the result from the Rietveld fit on the neutron diffraction data of TS samples ( $c_o \sim 66.7\%$ ,  $\langle u^2 \rangle = 0.208 \text{ \AA}^2$ ), and smaller than the result reported by *Nielsen* [5]. In this context it is interesting to mention the recent published work of *Bafle et al.* [30], who reports on neutron diffraction measurements of solid deuterium close to melting. The mean square displacement increases to  $\langle u^2 \rangle = 0.43 \text{ \AA}^2$  at  $T \sim 18.7 \text{ K}$ . The conclusion of *Bafle et al.* is the break down of the pseudoharmonic approach for solid deuterium close to the melting point.

## V. CONCLUSION

In this manuscript, we reported investigations on the density of states (DOS) of solid  $D_2$  for different o- $D_2$  concentrations with the powerful tool of neutron scattering. The experiments were performed at time-of-flight instruments at ILL, Grenoble and at FRM II, Garching. The DOS was extracted from the neutron data by applying the incoherent approximation. The results for the GDOS (generalized density of states) and the DOS show interesting details, which have not been published previously. One feature is the appearance of the  $J = 0 \mapsto 1$  in the DOS. The strength of this excitation increases with the o- $D_2$  concentration  $c_o$ . The DOS of solid  $D_2$  contains a strong phonon signal at 5 meV, but weak signals of optical phonons. Our results for the DOS indicate a smearing-out of the higher energy optical phonons for higher p- $D_2$  concentrations, which was also reported for solid hydrogen with high o- $H_2$  concentrations. The reason for this effect may be explained by the anharmonicity of the solid  $D_2$  crystal. Furthermore we see two-phonon processes at considerably low energies in our data (onset at 5 meV). Another new result is the appearance of a peak at  $\sim 12 \text{ meV}$  in the DOS of solid  $D_2$ . This peak increases with higher o- $D_2$  concentration, and could be explained by a coupled excitation of a phonon and a rotational transition, or by an possible incomplete separation of the one- and two-particle-contribution. This effect has to be further investigated. Our data of natural deuterium ( $c_o \sim 66.7\%$ ) are showing the rotational transition  $J = 1 \mapsto 2$ .

## **Acknowledgments**

This work was supported by the cluster of excellence "Origin and Structure of the Universe" Exc 153 and by the Maier-Leibnitz-Laboratorium (MLL) of Technische Universität München (TUM) and Ludwig-Maximilians-Universität (LMU). We thank T. Deuschle, H. Ruhland and E. Karrer-Müller for their help during the experiments and F. J. Hartmann for his helpful comments and notes concerning our manuscript.



- 
- [1] H. Saito, H. Nagao, K. Nishikawa, K. Kinugawa J. Chem. Phys. **119**, 953 (2003).
  - [2] H. Nielsen, Phys. Rev. B **7**, 1626 (1973).
  - [3] A. Driessen, E. van der Poll, I.F. Silvera, Phys. Rev. B **30**, 2517 (1984).
  - [4] I.F. Silvera, Rev. Mod. Phys. **52**, 393 (1980).
  - [5] H. Nielsen, B. Moeller, Phys. Rev. B **3**, 4383 (1971).
  - [6] S.N. Ishmaev, G.V. Kobelev, I.P. Sadikov, V.A. Sukhoparov, A.A. Chernyshov, A.S. Telepnev, B.A. Vindryaevskii, Y.L. Shitikov, Physica B **234-236**, 30 (1997).
  - [7] N.S. Sullivan, D. Zhou, C.M. Edwards, Cryogenics **30**, 734 (1990).
  - [8] C.Y. Liu, S.K. Lamoreaux, A. Saunders, D. Smith, A.R. Young, Nucl. Instrum. Methods A **508**, 257 (2003).
  - [9] A. Frei, A.R. Müller, D. Tortorella, E. Gutmiedl, F.J. Hartmann, S. Paul, R. Hackl, L. Tassini, O. Spieler, Nucl. Instrum. Methods A, submitted (2008).
  - [10] <http://www.ncnr.nist.gov/resources/n-lengths/>
  - [11] S.W. Lovesey, *Theory of Neutron Scattering from Condensed Matter* **1**, (Calderon, Oxford, 1984) 120.
  - [12] C.Y. Liu, A.R. Young, S.K. Lamoreaux, Phys. Rev. B **62**, R3581 (2000).
  - [13] G.L. Squires, *Introduction to the Theory of Thermal Neutron Scattering*, (Cambridge Univ. Press, Cambridge, 1978) 57-9.
  - [14] F.G. Mertens, W. Biem, Z. Phys. **250**, 273 (1972).
  - [15] H. Mutka, Nucl. Instrum. Methods A **338**, 144 (1994).
  - [16] T. Unruh, J. Neuhaus, W. Perty, Nucl. Instrum. Methods A **580**, 1414 (2007).
  - [17] <http://www.ncnr.nist.gov/equipment/oc.html>
  - [18] D.P. Weliky, T.J. Byers, K.E. Kerr, T. Momose, R.M. Dickson, T. Oka, Appl. Phys. B **59**, 265 (1994).
  - [19] G.W. Collins, W.G. Unites, E.R. Mapoles, T.P. Bernat, Phys. Rev. B **53**, 102 (1996).
  - [20] <http://www.ill.eu/computing-for-science/cs-software/all-software/lamp/>
  - [21] H. Schober, A. Tölle, B. Renker, R. Heid, F. Gompf, Phys. Rev. B **56**, 5937 (1997).
  - [22] V.F. Turchin, *Slow Neutrons* (Israel Program for Scientific Translations, Jerusalem, 1965).
  - [23] K.F. Mucker, P.M. Harris, David White, R.A. Erickson, J. Chem. Phys. **49**, 1922 (1968).

- [24] Z.-Ch. Yu, S.S. Malik, R. Golub, Z. Phys. B **62**, 137 (1985).
- [25] V.F. Sears, Adv. Phys. **24**, 1 (1975).
- [26] G.E. Bacon, *Neutron Diffraction* , (Oxford, University Press,1962).
- [27] A. Bickermann, H. Spitzer, H. Stiller, H. Meyer, R.E. Lechner, F. Volino, Z. Phys. B **31**, 345 (1978).
- [28] D. Colognesi, M. Celli, M. Zoppi, J. Chem. Phys. **120**, 5657 (2004).
- [29] J. Van Kranendonk and V.F. Sears, Can. J. Phys **44**, 313 (1966).
- [30] U. Bafle, F. Becherini, D. Colognesi, M. Zoppi, Phys. Rev. B **77**, 224302-1 (2008).

## Figure captions:

Fig. 1:

Sketch of the D<sub>2</sub> sample cell.

Fig. 2:

D<sub>2</sub> phase diagram with different process paths studied: a) liquefaction from the gas, b) solidification from liquid, c) sublimation at high temperature, d) direct condensation.

Fig. 3:

Sketch of the para-to-ortho converter [9]. The copper converter cup is filled with OXISORB grain, and mounted on the cold-finger of the cooling machine.

Fig. 4:

Pictures of solid deuterium samples for different freezing procedures.

Crystals from the liquid phase are transparent, if they are frozen slowly, while a fast freezing/cool down (within minutes) leads to a non-transparent solid.

- a) solid deuterium slowly frozen from the liquid phase (LS),
- b) solid deuterium slowly frozen from the gas phase (GS),
- c) solid deuterium fast freezing/cool down from the liquid phase (TS).

Fig. 5:

Generalized density of states (GDOS) of natural deuterium ( $c_o = 66.7\%$ ):

liquid D<sub>2</sub> ( $\square$ ) at  $T = 21$  K, solid D<sub>2</sub> ( $\triangle$ ), rapidly frozen out from the liquid phase and fast cooled down, solid D<sub>2</sub> ( $\circ$ ), slowly frozen out from the liquid phase, solid D<sub>2</sub> ( $\star$ ), slowly frozen out from the gas phase. All solids have a temperature of  $T = 4$  K. Peaks are convoluted with IN4 energy resolution curve: Normalized by  $\int_0^\infty GDOS(E) \cdot dE = 1$ .

Each GDOS is separated by a shift of 0.1.

Fig. 6:

Generalized density of states (GDOS) of converted deuterium ( $c_o = 95\%$ ):

liquid D<sub>2</sub> ( $\square$ ) at  $T = 20$  K, solid D<sub>2</sub> ( $\triangle$ ), slowly frozen out from the liquid phase, solid D<sub>2</sub> ( $\circ$ ), slowly frozen out from the gas phase, solid D<sub>2</sub> ( $\star$ ), frozen out at the melting point and slowly cooled down. All solids have a temperature of  $T = 4$  K. Peaks are convoluted with

IN4 energy resolution curve: Normalized by  $\int_0^\infty GDOS(E) \cdot dE = 1$ .

Each GDOS is separated by a shift of 0.1.

Fig. 7:

Dynamical neutron scattering cross section of solid D<sub>2</sub> for  $c_o = 66.7\%$  ( $\square$ ) and  $c_o = 98\%$  ( $\circ$ ) at  $T = 7$  K. Data from the TOFTOF measurements.

Fig. 8:

Neutron diffraction pattern data of fast frozen solid D<sub>2</sub> (TS) for  $c_o = 66.7\%$  ( $\triangle$ ) at  $T = 9.5$  K and comparison with a Rietveld fit (solid line) for powder like hcp solid D<sub>2</sub>. Data from the TOFTOF measurements.

Fig. 9:

Dynamic neutron scattering cross section of solid D<sub>2</sub> for  $c_o = 66.7\%$  and  $c_o = 98\%$  at  $T = 7$  K.

Comparison of data with calculated neutron cross sections.

The one-particle contribution is shown by the dashed line, the two-particle contribution by the dotted line, and the three-particle contribution by the dash-dotted line. Contribution of multiple scattering is shown by the dot-dot-dash line. Data from the TOFTOF measurements.

Fig. 10:

a) One-particle density of states of solid D<sub>2</sub> for  $c_o = 66.7\%$  ( $\circ$ ),  $c_o = 98\%$  ( $\square$ ) at  $T = 7$  K.

b) Comparison of de-convoluted DOS with data ( $\star$ ) from *Yu et al.* [24].

The DOS (part b)) are de-convoluted with the FWHM of the elastic peak of  $d\sigma/dE$ .

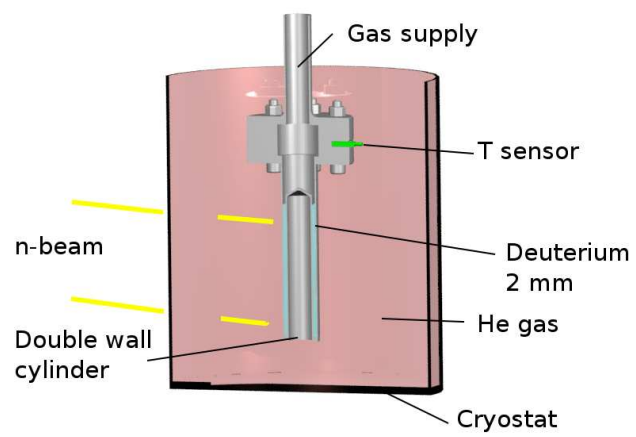


FIG. 1:  
Sketch of the D<sub>2</sub> sample cell.

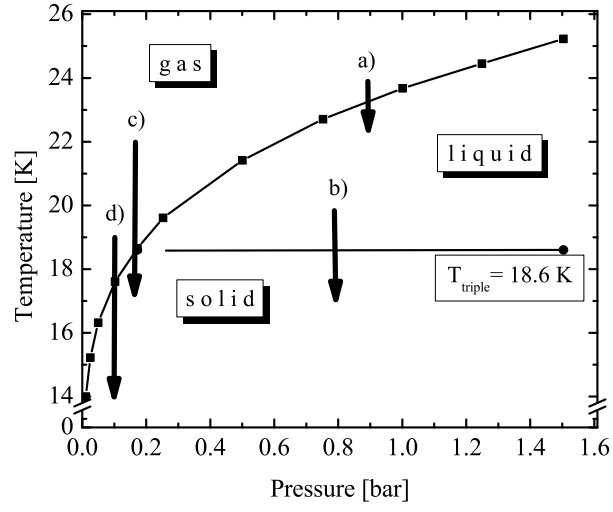


FIG. 2:

D<sub>2</sub> phase diagram with different process paths studied: a) liquefaction from the gas, b) solidification from liquid, c) sublimation at high temperature, d) direct condensation.

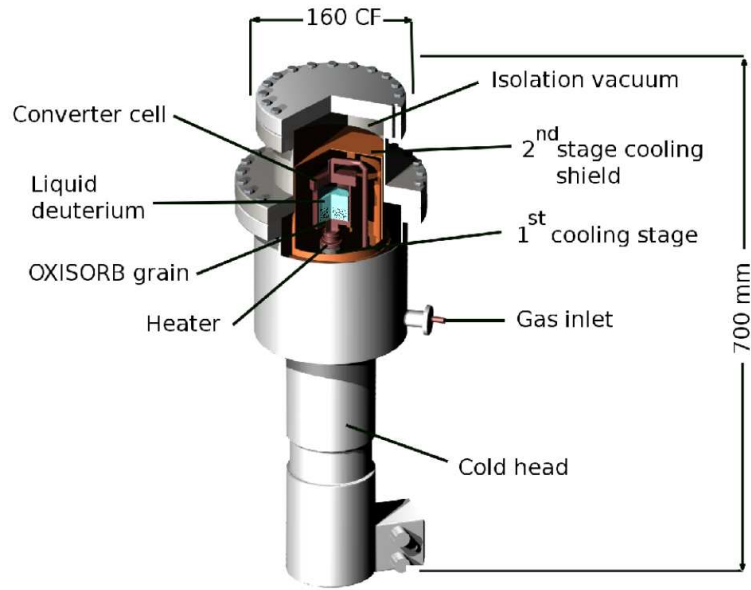


FIG. 3:

Sketch of the para-to-ortho converter [9]. The copper converter cup is filled with OXISORB grain, and mounted on the cold-finger of the cooling machine.

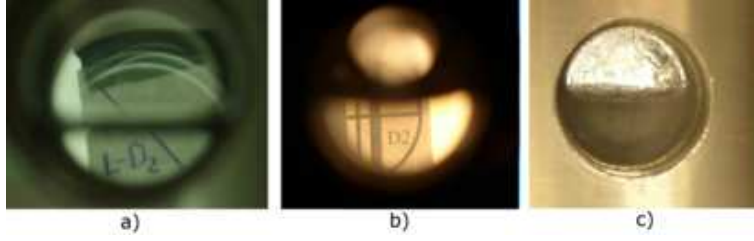


FIG. 4:

Pictures of solid deuterium samples for different freezing procedures.

Crystals from the liquid phase are transparent, if they are frozen slowly, while a fast freezing/cool down (within minutes) leads to a non-transparent solid.

a) solid deuterium slowly frozen from the liquid phase (LS),

b) solid deuterium slowly frozen from the gas phase (GS),

c) solid deuterium fast freezing/cool down from the liquid phase (TS).



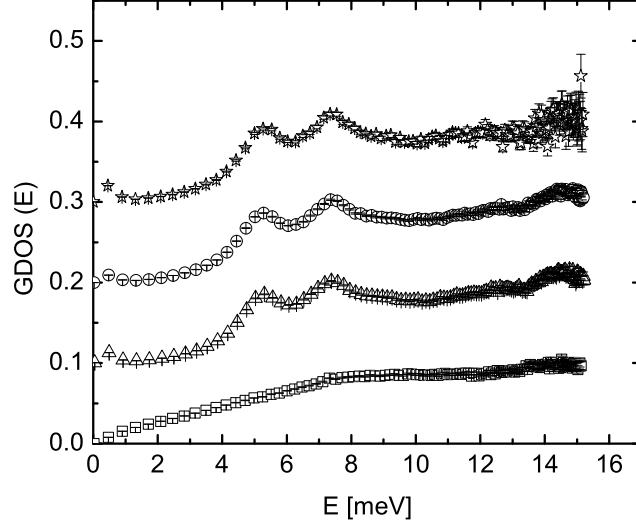


FIG. 5:

Generalized density of states (GDOS) of natural deuterium ( $c_o = 66.7\%$ ):

liquid  $D_2$  ( $\square$ ) at  $T = 21$  K, solid  $D_2$  ( $\triangle$ ), rapidly frozen out from the liquid phase and fast cooled down, solid  $D_2$  ( $\circ$ ), slowly frozen out from the liquid phase, solid  $D_2$  ( $\star$ ), slowly frozen out from the gas phase. All solids have a temperature of  $T = 4$  K. Peaks are convoluted with the IN4

energy resolution curve: Normalized by  $\int_0^\infty GDOS(E) \cdot dE = 1$ .

Each GDOS is separated by a shift of 0.1.

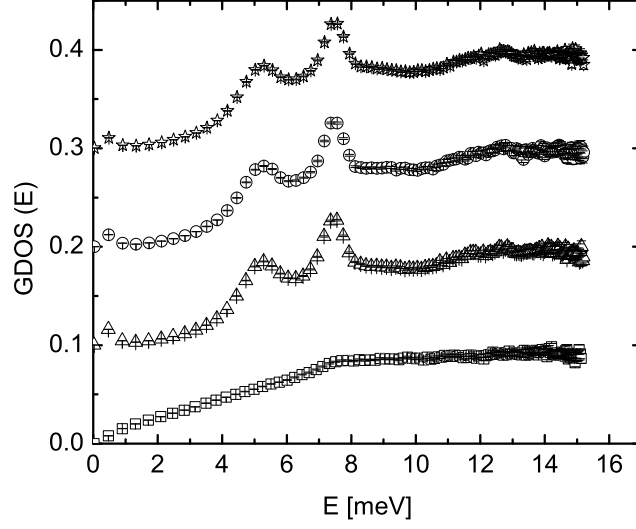


FIG. 6:

Generalized density of states (GDOS) of converted deuterium ( $c_o = 95\%$ ):  
 liquid  $D_2$  ( $\square$ ) at  $T = 20$  K, solid  $D_2$  ( $\triangle$ ), slowly frozen out from the liquid phase, solid  $D_2$  ( $\circ$ ),  
 slowly frozen out from the gas phase, solid  $D_2$  ( $\star$ ), frozen out at the melting point and slowly  
 cooled down. All solids have a temperature of  $T = 4$  K. Peaks are convoluted with IN4 energy  
 resolution curve: Normalized by  $\int_0^\infty GDOS(E) \cdot dE = 1$ .

Each GDOS is separated by a shift of 0.1.

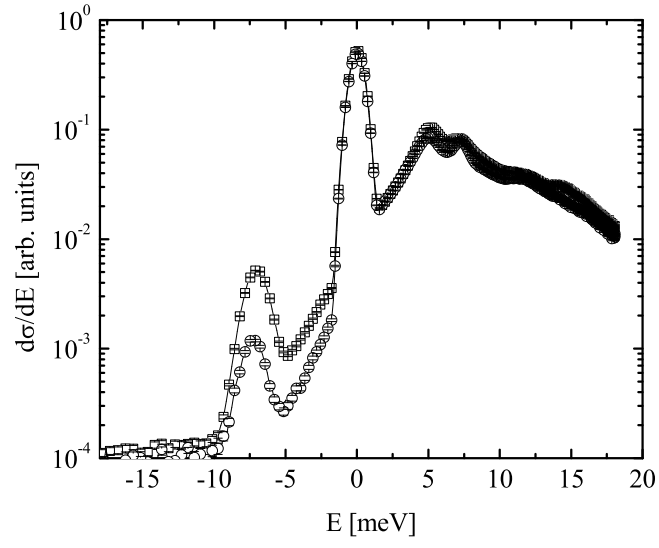


FIG. 7:

Dynamical neutron scattering cross section of solid  $D_2$  for  $c_o = 66.7\%$  ( $\square$ ) and  $c_o = 98\%$  ( $\circ$ ) at  $T = 7$  K. Data from the TOFTOF measurements.

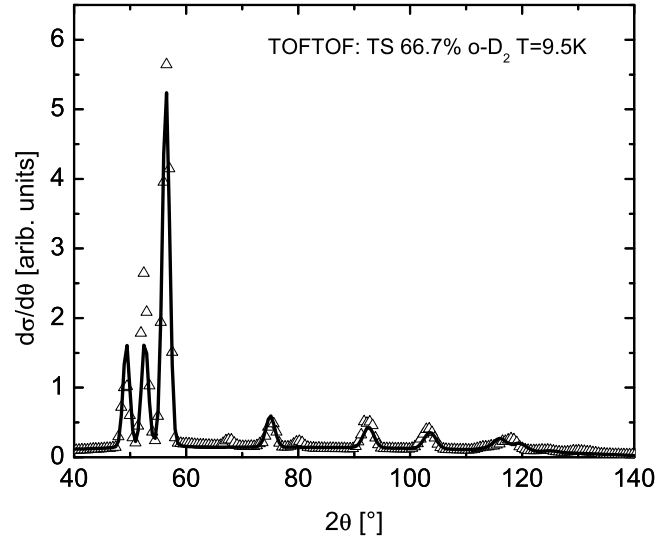


FIG. 8:

Neutron diffraction pattern data of fast frozen solid D<sub>2</sub> (TS) for  $c_o = 66.7\%$  ( $\triangle$ ) at  $T = 9.5$  K and comparison with a Rietveld fit (solid line) for powder like hcp solid D<sub>2</sub>. Data from the TOFTOF measurements.

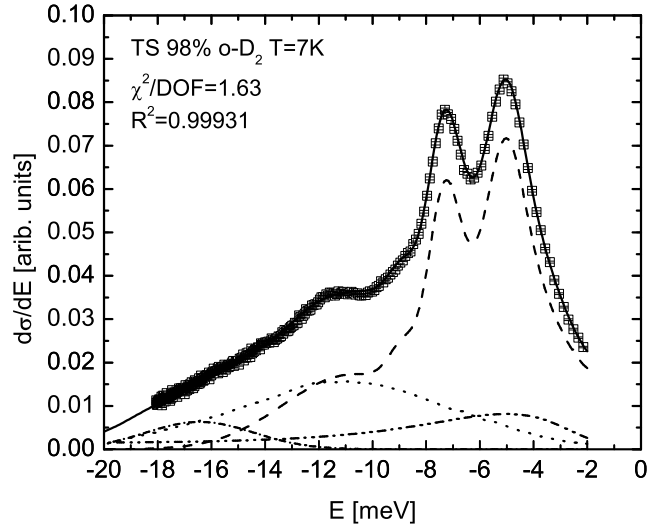
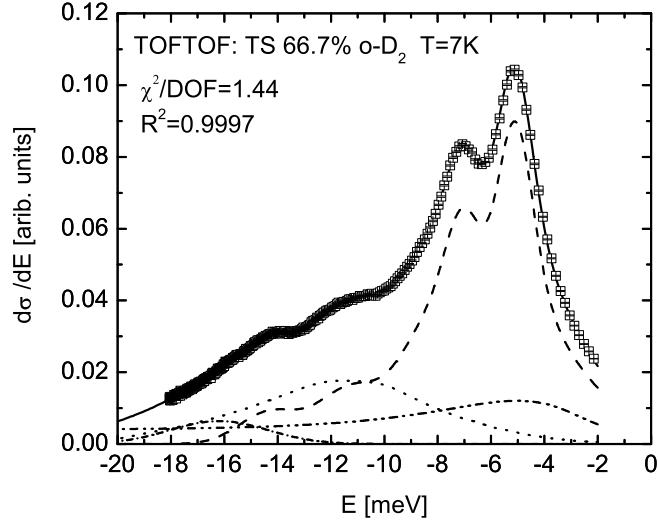


FIG. 9:

Dynamic neutron scattering cross section of solid  $D_2$  for  $c_o = 66.7\%$  and  $c_o = 98\%$  at  $T = 7$  K.

Comparison of data with calculated neutron cross sections.

The one-particle contribution is shown by the dashed line, the two-particle contribution by the dotted line, and the three-particle contribution by the dash-dotted line. Contribution of multiple scattering is shown by the dot-dot-dash line. Data from the TOFTOF measurements.

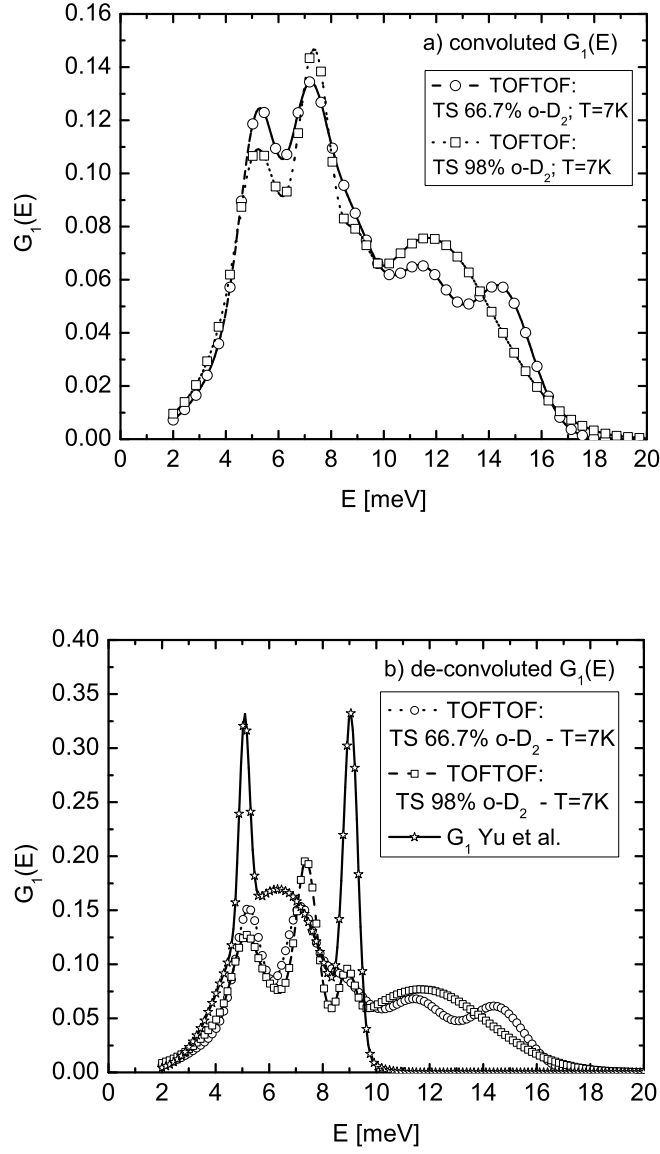


FIG. 10:

a) One-particle density of states of solid  $D_2$  for  $c_o = 66.7\%$  ( $\circ$ ),  $c_o = 98\%$  ( $\square$ ) at  $T = 7$  K.

b) Comparison of de-convoluted DOS with data ( $\star$ ) from *Yu et al.* [24].

The DOS (part b)) are de-convoluted with the FWHM of the elastic peak of  $d\sigma/dE$ .